A super tiny quartz tuning fork-based light-induced thermoelastic spectroscopy sensing

Shunda Qiao,[1] Pengze Ma,[2] Viktor Tsepelin,[3] Guowei Han,[4] Jinxing Liang,[5] Wei Ren,[6] Huadan Zheng,[2,7] Yufei Ma [1,*]

[1] *National Key Laboratory of Science and Technology on Tunable Laser, Harbin Institute of Technology, Harbin 150001, China*
[2] *Key Laboratory of Optoelectronic Information and Sensing Technologies of Guangdong Higher Education Institutes, Jinan University, Guangzhou, 510632, China*
[3] *Department of Physics, Lancaster University, Lancaster LA1 4YB, UK*
[4] *Engineering Research Center for Semiconductor Integrated Technology, Institute of Semiconductors, Chinese Academy of Sciences, Beijing 100083, China*
[5] *Key Laboratory of Micro-Inertial Instrument and Advanced Navigation Technology, Ministry of Education, School of Instrument Science and Engineering, Southeast University, Nanjing 210096, China*
[6] *Department of Mechanical and Automation Engineering, The Chinese University of Hong Kong, New Territories, Hong Kong SAR, China*
[7] *zhenghuadan@jnu.edu.cn*
**Corresponding author: mayufei@hit.edu.cn*

Received XX Month XXXX; revised XX Month, XXXX; accepted XX Month XXXX; posted XX Month XXXX (Doc. ID XXXXX); published XX Month XXXX

In this paper, a sensitive light-induced thermoelastic spectroscopy (LITES) based trace gas sensor by exploiting a super tiny quartz tuning fork (QTF) was demonstrated. The prong length and width of this QTF are 3500 μm and 90 μm, respectively, which determines a resonant frequency of 6.5 kHz. The low resonant frequency is beneficial to increase the energy accumulation time in LITES sensor. The geometric dimension of QTF in micrometer scale is advantageous to obtain a great thermal expansion and thus can produce a strong piezoelectric signal. The temperature gradient distribution of the super tiny QTF was simulated based on the finite element analysis and is higher than that of the commercial QTF with 32.768 kHz. Acetylene (C_2H_2) was used as the analyte. Under the same conditions, the use of the super tiny QTF achieved a 1.64 times signal improvement compared with the commercial QTF. The system shows excellent long-term stability according to the Allan deviation analysis, and a minimum detection limit (MDL) would reach 190 ppb with an integration time of 220 s. © 2022 Optical Society of America

http://dx.doi.org/10.1364/OL.99.099999

Laser absorption spectroscopy-based trace gas sensing has attracted much interest in recent years due to its excellent "finger-print" identifying characteristics and high detection sensitivity [1-7]. With the first proposal of quartz-enhanced photoacoustic spectroscopy (QEPAS) in time [8], quartz tuning fork (QTF) was firstly introduced into the laser spectroscopy based trace gas detection techniques. In QEPAS, QTF is utilized as an acoustic wave transducer. Compared with the microphone used in traditional photoacoustic spectroscopy (PAS), QTF has a higher quality factor, narrower response frequency bandwidth and smaller geometric size [9,10]. Therefore, it is beneficial for the sensing system to get a high signal level, be immune to background noise and realize miniaturization and integration [11-15]. However, in QEPAS, to detect the photoacoustic signal, a QTF must be exposed to the target analyte, which means QEPAS is a contact measurement method. When the acid or corrosive gases exist in the detection environment [16,17], QTF will be corroded with long-term exposure and finally reduces the lifetime of the sensors.

In 2018, a novel QTF-based trace gas detection technique named light-induced thermoelastic spectroscopy (LITES) was reported by Ma et al [18]. Different from the detection mechanisms of QEPAS, a QTF is utilized as a light-thermal detector in the LITES system. After being absorbed by the target gas, the laser hits the surface of QTF. The residual laser energy is converted into thermal energy because of the absorption of quartz material, which results in the thermoelastic expansion of QTF [19-22]. By modulating the laser, the periodic thermoelastic deformation forces the QTF to generate mechanical motion. This motion will be enhanced when its frequency is consistent with the resonant effect of QTF [23]. According to the piezoelectric effect, an electrical signal containing gas concentration information is produced [24,25]. In LITES, QTF does not need to be placed in the analyte, which means it is a non-contact measurement method. Therefore, such a technique not only maintains the advantages of QEPAS but also eliminates the risk of sensor failure due to the corrosion of QTF. Up to now, LITES has been used to detect various gases [26-30].

QTF, as the core element of QEPAS and LITES, can effectively improve detection performance by optimizing its parameters. For a QTF-based sensor, the resonant frequency of QTF determines the modulation period of the system [31]. A higher frequency of QTF will lead to a

shorter period which corresponds to a shorter energy accumulation time and ultimately limits the sensor performance. At present, some different QTFs with a low frequency of <10 kHz have been designed and used in gas sensing [32-38]. Compared with the commonly used standard QTF with a resonant frequency of ~32 kHz, these low-frequency QTFs achieve a better detection sensitivity. In addition, in LITES, the light-induced thermoelastic signal is positively correlated with the temperature gradient amplitude of the QTF. Under the same excitation conditions, when the boundary temperature is constant, the smaller geometric size of QTF will increase the temperature gradient amplitude of QTF, which is finally beneficial to produce a stronger LITES signal.

In this paper, a sensitive LITES sensor based on a super tiny QTF with a low resonant frequency was demonstrated. The prong length and width of the used QTF are 3500 μm and 90 μm, respectively, which determines a resonant frequency of 6.5 kHz. The spacing between the two prongs of the QTF is 80 μm. The temperature gradient on the surface of the super tiny QTF was simulated and compared with that of the standard commercial QTF. In addition, the detection performance of the LITES sensing system was also compared when these two different QTFs were used. Acetylene (C_2H_2) was chosen as the target analyte. By employing the Allan deviation analysis, the long-term stability of the system was verified.

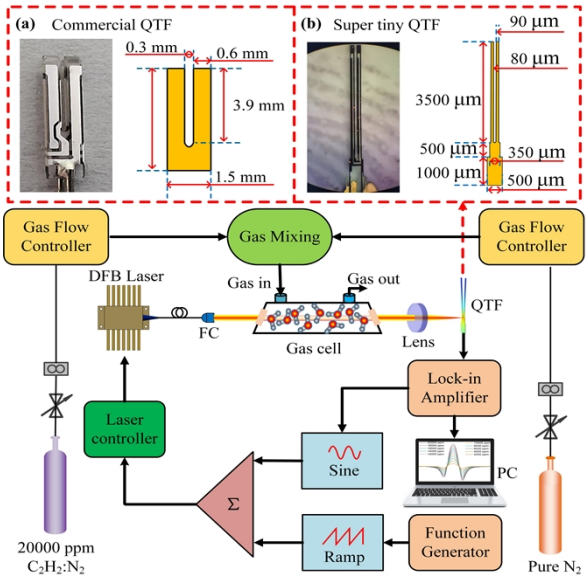

Fig. 1. Schematic configuration of the C_2H_2-LITES sensor. DFB: distribute feedback; FC: fiber collimator; QTF: quartz tuning fork; PC: personal computer. (a) Diagram of the standard commercial QTF. (b) Diagram of the super tiny QTF.

A schematic of the super tiny QTF-based LITES sensor system is depicted in Fig. 1. According to the HITRAN 2016 database, an absorption line of C_2H_2 located at 1530.37 nm (6534.37 cm^{-1}) was selected to investigate the sensor performance. A tunable continuous-wave (CW) distributed feedback (DFB) diode laser emitting at 1.53 μm was used as the excitation source. When the operating temperature of the laser was set at 22 °C, the CW-DFB laser can reach the selected absorption line with the driving current of 82 mA. The laser beam was collimated with a fiber collimator (FC) and then focused on the surface of the QTF after passing through the target gas. The optical length of the gas cell was 20 cm. The super tiny QTF was custom made from a 75 μm -thick wafer. Electrical connections were made by soldering silver wire to the contact pads. A picture of the employed two QTFs including a standard commercial QTF and the super tiny QTF are shown in Fig. 1(a) and Fig. 1 (b), respectively. The prong length and width of the super tiny QTF are 3500 μm and 90 μm, respectively. And the spacing between the two prongs is 80 μm. As the size of the super tiny QTF is in the micrometer scale, the actual picture was obtained by using an optical microscope. To reduce the influence of the background noise, wavelength modulation spectroscopy (WMS) and the 2nd harmonic demodulation techniques were utilized in the system to reduce the background noise. The laser wavelength was tuned across the gas absorption line with a ramp wave provided by a function generator. Moreover, a sine wave generated from a lock-in amplifier was used to modulate the laser wavelength and as the reference signal for demodulation. The integration time of the system was 200 ms which corresponded to a detection bandwidth of 345.4 mHz.

The thermal expansion of QTF is mainly caused by its own non-uniform temperature distribution. And the thermal stress is proportional to the temperature gradient. Therefore, the amplitude of the temperature gradient determines the thermal expansion strength of the QTF, which finally determines the LITES signal level. The temperature gradient distribution of the horizontal line at the position of the laser hit on the surface of QTF is calculated using the finite element analysis method with the COMSOL software. Two different QTFs of the super tiny QTF and a standard commercial QTF were compared. During the calculations, the physical model was established according to the actual size of the QTFs as shown in Fig. 1(a) and Fig. 1(b). Two physical fields of solid heat transfer and solid mechanics were used. The results of the simulated calculation for the two different QTFs are shown in Fig. 2(a) and Fig. 2(b), respectively. Under the same excitation intensity, compared to the commercial QTF, the super tiny QTF generated a higher temperature gradient amplitude. Therefore, a stronger thermal stress will be produced and result in a larger thermal expansion, which is obviously beneficial to generate a higher LITES signal.

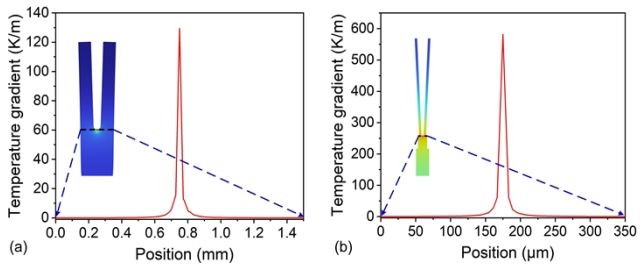

Fig. 2. The temperature gradient distribution of the QTFs with the same excitation intensity. (a) The commercial QTF. (b) The super tiny QTF.

To determine the modulation frequency of the system, the resonant frequency of the QTFs was measured at first. The frequency response curve of the two different QTFs is shown in Fig. 3(a). The data were normalized and fitted with a Lorentz function. According to the results of the measurement, the resonant frequency of the super tiny QTF and the standard commercial QTF were f_1=6531.21 Hz and f_2=32759.90 Hz, respectively. Furthermore, the response bandwidth was determined as Δf_1= 8.27 Hz and Δf_2=2.97 Hz, respectively. The modulation depth is an important parameter for the WMS technique which has a significant influence on the level of the LITES signal. Therefore, the current modulation depth of the sensing system with the two different QTFs was optimized. The signal amplitude as a function of current

modulation depth is depicted in Fig. 3(b). The measured results show that the LITES signal reached the maximum when the current modulation depth was 15.45 mA for the super tiny QTF and 20.64 mA for the standard commercial QTF, respectively. During the experiment, the laser needs to be modulated with different frequencies according to the resonant frequencies of the two QTFs. The modulation performance of the laser is dissimilar at different modulation frequencies, which is the main reason for the different current modulation depths for the two QTFs.

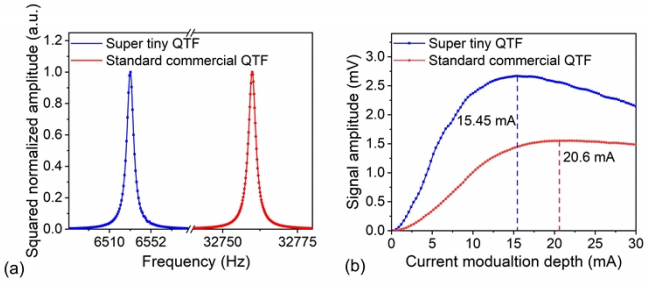

Fig. 3. (a) Frequency response curve for the super tiny QTF (blue line) and the commercial QTF (red line), respectively. (b) LITES signal amplitude as a function of the current modulation depth for the super tiny QTF (blue line) and the commercial QTF (red line), respectively.

Under the same experimental conditions, the 2*f* LITES signal detected by the two different QTFs was compared with a 2% C_2H_2:N_2 gas mixture. As shown in Fig. 4(a), the 2*f* signal amplitude was 2.67 mV and 1.64 mV for the super tiny QTF and standard commercial QTF, respectively. The LITES signal amplitude with the super tiny QTF improved 1.64 times compared to the commercial QTF. Such an improvement is mainly due to the low resonant frequency and small geometric size of the super tiny QTF, which is beneficial for increasing the energy accumulation time of the sensing system and strengthening the thermal stress of itself. The background noise of the LITES sensing system by utilizing the two different QTFs was also compared. Fill the gas cell with the pure N2 and lock the laser wavelength at the absorption peak of the target line. Then, the 2*f* LITES signal amplitude was monitored continuously for 300 s. The results of the measurement are shown in Fig. 4(b). The 1σ noise of the LITES sensor system was 323 nV and 364 nV for the super tiny QTF and commercial QTF, respectively, which produced a minimum detection limit (MDL) of 2.41 ppm and 4.43 ppm, accordingly.

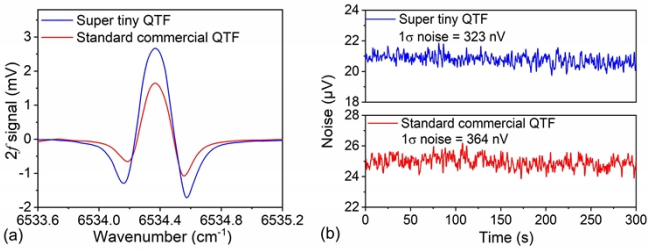

Fig. 4. (a) Comparison of the 2*f* LITES signals measured by the two different QTFs for a 2% C_2H_2:N_2 gas mixture. (b) System noise measured with the two different QTFs with a 200 ms integration time.

The gas concentration response of the LITES sensing system utilizing the super tiny QTF was investigated. A 2% C_2H_2:N_2 gas mixture was diluted with pure N_2 by employing two gas flow controllers to produce different target concentrations. The 2*f* LITES signal with each C_2H_2 concentration was measured and is shown in Fig. 5(a). The signal peak values as a function of gas concentrations are depicted in Fig. 5(b). The data were fitted by using a linear function and the R-squared value reached 0.99, which indicated an excellent linear response of gas concentration for the reported sensor system.

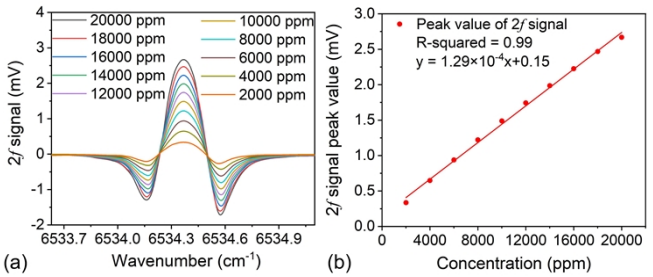

Fig. 5. (a) 2*f* LITES signal with different gas concentrations when the super tiny QTF was used. (b) 2*f* signal peak values as a function of gas concentrations.

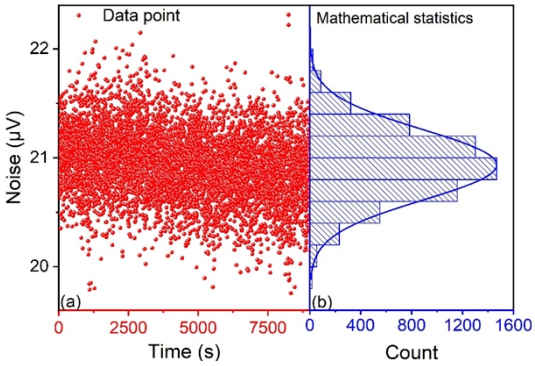

Fig. 6. (a) Continuous monitoring of signal amplitude for more than 2.5 hours with the gas cell filled with pure N_2. (b) Mathematical statistic of the data points.

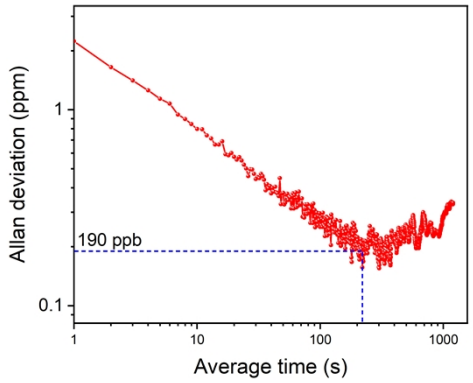

Fig. 7. Allan deviation for the super tiny QTF-based C_2H_2-LITES sensor system.

The long-term stability of the super tiny QTF-based LITES sensor system was evaluated by using the Allan deviation analysis. The signal amplitude was monitored continuously for more than 2.5 hours with the gas cell filled with pure N_2. The mathematical statistics proceeded to the data point. The results of the measurement and statistics are shown in Fig. 6(a) and 6(b), respectively. It can be seen from the results that the data presents a good Gaussian distribution, which means the white noise was dominant. Based on the obtained data, the result of the Allan deviation analysis is depicted in Fig. 7. It showed that the reported sensor system had excellent stability. When the integration time of the system was 220 s, an MDL of 190 ppb for the detection of C_2H_2 could be achieved.

In conclusion, a sensitive LITES sensor exploiting a super tiny QTF with low resonant frequency was demonstrated. The prong length and width of the QTF are 3500 μm and 90 μm, respectively, and the gap between the two prongs of the QTF is 80 μm, all of which determines the resonant frequency to be 6.5 kHz. By using the finite element analysis method, the temperature gradient distribution of the super tiny QTF was simulated and compared to that of the standard commercial one. The super tiny QTF showed a greater temperature gradient than that of the commercial QTF with the same excitation source, which means this tiny QTF has a stronger thermal expansion strength. In the experimental verification section, a LITES sensor based on this tiny QTF was built and C_2H_2:N_2 gas mixture was used as the analyte. Compared with the commercial QTF the signal level achieved a 1.64 times improvement when the super tiny QTF was adopted, and an MDL of 2.41 ppm was obtained at the conditions of 200 ms integration time. It was verified that the reported sensor achieved an excellent linear response to the C_2H_2 concentration. Furthermore, the long-term stability of the sensing system was also investigated by employing the Allan deviation analysis, and an MDL of 190 ppb could be obtained with an integration time of 220 s. The reported sensor proved the advantage of a small-size low-frequency QTF in the LITES technique, and the sensor performance can be improved by further optimizing the parameters of the QTFs.

Funding. National Natural Science Foundation of China (Grant No. 62275065, 62022032, 61875047 and 61505041), Fundamental Research Funds for the Central Universities.

Disclosures. The authors declare no conflicts of interest.

Data availability. Data underlying the results presented in this paper are not publicly available at this time but may be obtained from the authors upon reasonable request.

References

1. Y. F. Ma, R. Lewicki, M. Razeghi, and F. K. Tittel, Opt. Express **21**, 1008–1019 (2013).
2. Z. Zhang, F. Zhang, B. Xu, H. Xie, B. Fu, X. Lu, N. Zhang, S. Yu, J. Yao, and Y. Cheng, Ultrafast Science **2022**, 9761458 (2022).
3. X. N. Liu, and Y. F. Ma, Sensors **22**, 6095 (2022).
4. Z. L. Li, Z. Wang, Y. Qi, W. Jin, and W. Ren, Sensor. Actuat. B-Chem. **248**, 1023–1028 (2017).
5. Y. Fu, J. Cao, K. Yamanouchi, and H. Xu, Ultrafast Science **2022**, 9867028 (2022).
6. P. Patimisco, G. Scamarcio, F. K. Tittel, and V. Spagnolo, Sensors **14**, 6165–6206 (2014).
7. Y. H. Liu, and Y. F. Ma, Chin. Opt. Lett. **21**, 033001 (2023).
8. A. A. Kosterev, Y. A. Bakhirkin, R. F. Curl, and F. K. Tittel, Opt. Lett. **27**, 1902–1904 (2002).
9. M. Mordmüller, M. Köhring, W. Schade, and U. Willer, Appl. Phys. B **119**, 111–118 (2015).
10. L. Dong, A. A. Kosterev, D. Thomazy, and F. K. Tittel, Appl. Phys. B **100**, 627–635 (2010).
11. H. Y. Lin, H. D. Zheng, B. Y. Antonio Z. Montano, H. P. Wu, M. Giglio, A. Sampaolo, P. Patimisco, W. G. Zhu, Y. C. Zhong, L. Dong, R, F. Kan, J. H. Yu, and V. Spagnolo, Photoacoustics **25**, 100321 (2022).
12. K. Liu, X. Y. Guo, H. M. Yi, W. D. Chen, W. J. Zhang, and X. M. Gao, Opt. Lett. **34**, 1594–1596 (2009).
13. P. Patimisco, A. Sampaolo, L. Dong, F. K. Tittel, and V. Spagnolo, Appl. Phys. Rev. **5**, 011106 (2018).
14. H. H. Lv, H. D. Zheng, Y. H. Liu, Z. F. Yang, Q. Wu, H. Y. Lin, B. Y. Antonio Z. Montano, W. G. Zhu, J. H. Yu, R. F. Kan, Z. Chen, and F. K. Tittel, Opt. Lett. **46**, 3917–3920 (2021).).
15. T. Milde, M. Hoppe, H. Tatenguem, M. Mordmüller, J. O'Gorman, U. Willer, W. Schade, and J. Sacher, Appl. Optics **57**, C120–C127 (2018).
16. Y. F. Ma, Y. He, X. Yu, C. Chen, R. Sun, and F. K. Tittel, Sensor. Actuat. B-Chem **233**, 388–393 (2016).
17. H. P. Wu, A. Sampaolo, D. Lei, P. Patimisco, X. L. Liu, H. D. Zheng, X. K. Yin, W. G. Ma, L. Zhang, W. B. Yin, V. Spagnolo, S. T. Jia, and F. K. Tittel, Appl. Phys. Lett. **107**, 111104 (2015).
18. Y. F. Ma, Y. He, Y. Tong, X. Yu, and F. K. Tittel, Opt. Express **26**, 32103–32110 (2018).
19. X. N. Liu, S. D. Qiao, and Y. F. Ma, Opt. Express **30**, 1304–1313 (2022).
20. S. D. Russo, A. Zifarelli, P. Patimisco, A. Sampaolo, T. T. Wei, H. P. Wu, L. Dong, and V. Spagnolo, Opt. Express **28**, 19074–19084 (2020).
21. Y. F. Ma, Y. Q. Hu, S. D. Qiao, Z. T. Lang, X. N. Liu, Y. He, and V. Spagnolo, Photoacoustics **25**, 100329 (2022).
22. Q. D. Zhang, J. Chang, Z. H. Cong, and Z. L. Wang, Sens. Actuators A. **299**, 111629 (2019).
23. Z. T. Lang, S. D. Qiao, Y. He, and Y. F. Ma, Photoacoustics **22**, 100272 (2021).
24. X. N. Liu, and Y. F. Ma, Chin. Opt. Lett. **20**, 031201 (2022).
25. T. T. Wei, A. Zifarelli, S. Dello Russo, H. P. Wu, G. Menduni, P. Patimisco, A. Sampaolo, V. Spagnolo, and L. Dong, Appl. Phys. Rev. **8,** 041409 (2021).
26. S. D. Qiao, A. Sampaolo, P. Patimisco, V. Spagnolo, and Y. F. Ma, Photoacoustics **27**, 100381 (2022).
27. X. N. Liu, S. D. Qiao, G. W. Han, J. X. Liang, and Y. F. Ma, Photoacoustics **28**, 100422 (2022).
28. L. Hu, C. T. Zheng, M. H. Zhang, K. Y. Zheng, J. Zheng, Z. W. Song, X. Y. Li, Y. Zhang, Y. D. Wang, and F. K. Tittel, Photoacoustics **21**, 100230 (2021).
29. Y. M. Ma, C. T. Zheng, L. Hu, K. Y. Zheng, F. Song, Y. Zhang, Y D. Wang, and F. K. Tittel, Sensor. Actuat. B-Chem. **370**, 132429 (2022).
30. L. Hu, C. T. Zheng, Y. Zhang, J. Zheng, Y. D. Wang, F. K. Tittel, Opt. Lett. **45**, 1894-1897 (2020).
31. Y. F. Ma, Y. He, L. G. Zhang, X. Yu, J. B. Zhang, R. Sun, and Frank K. Tittel, Appl. Phys. Lett. **110**, 031107 (2017).
32. Q. Z. Wang, W. R.Wang, P. Patimisco, A. Sampaolo, and V. Spagnolo, Sensor. Actuat. B-Chem, **268**, 512–518 (2018).
33. Y. F. Ma, S. D. Qiao, P. Patimisco, A. Sampaolo, Y. Wang, and F. K. Tittel, and V. Spagnolo, Appl. Phys. Lett. **116**, 061101 (2020)
34. Z. J. Shang, S. Z. Li, B. Li, H. P. Wu, A. Sampaolo, P. Patimisco, V. Spagnolo, and L. Dong, Photoacoustics **26**, 100363 (2022).
35. Z. Wang, Q. Wang, H. Zhang, S. Borri, I. Galli, A. Sampaolo, P. Patimisco, V. L. Spagnolo, P. De Natale, and W. Ren. Photoacoustics **27**, 100387 (2022).
36. Y. F. Ma, Y. He, P. Patimisco, A. Sampaolo, S. D. Qiao, X. Yu, F. K. Tittel, and V. Spagnolo, Appl. Phys. Lett. **116**, 011103 (2020).
37. P. Patimisco, A. Sampaolo, H. Zheng, L. Dong, F. K. Tittel, and V. Spagnolo, Adv. Phys. X **2**, 169–187 (2017).
38. S. Dello Russo, A. Sampaolo, P. Patimisco, G. Menduni, M. Giglio, C. Hoelzl, V. M. N. Passaro, H. P. Wu, L. Dong, and V. Spagnolo, Photoacoustics **21**, 100227 (2021).

FULL REFERENCES

1. Y. F. Ma, R. Lewicki, M. Razeghi, and F. K. Tittel, "QEPAS based ppb-level detection of CO and N_2O using a high power CW DFB-QCL," Optics Express **21**, 1008–1019 (2013).
2. Z. Zhang, F. Zhang, B. Xu, H. Xie, B. Fu, X. Lu, N. Zhang, S. Yu, J. Yao, and Y. Cheng, "High-sensitivity gas detection with air-lasing-assisted coherent Raman spectroscopy," Ultrafast Science **2022**, 9761458 (2022).
3. X. N. Liu, and Y. F. Ma, "Tunable diode laser absorption spectroscopy based temperature measurement with a single diode laser near 1.4 μm," Sensors **22**, 6095 (2022).
4. Z. L. Li, Z. Wang, Y. Qi, W. Jin, and W. Ren, "Improved evanescent-wave quartz-enhanced photoacoustic CO sensor using an optical fiber taper," Sensors and Actuators B-Chemical **248**, 1023–1028 (2017).
5. Y. Fu, J. Cao, K. Yamanouchi, and H. Xu, "Air-laser-based standoff coherentRaman spectrometer," Ultrafast Science **2022**, 9867028 (2022).
6. P. Patimisco, G. Scamarcio, F. K. Tittel, and V. Spagnolo, "Quartz-enhanced photoacoustic spectroscopy: a review," Sensors **14**, 6165–6206 (2014).
7. Y. H. Liu, and Y. F. Ma, Advances in multipass cell for absorption spectroscopy-based trace gas sensing technology," Chinese Optics Letters **21**, 033001 (2023).
8. A. A. Kosterev, Y. A. Bakhirkin, R. F. Curl, and F. K. Tittel, "Quartz-enhanced photoacoustic spectroscopy," Optics Letters **27**, 1902–1904 (2002).
9. M. Mordmüller, M. Köhring, W. Schade, and U. Willer, "An electrically and optically cooperated QEPAS device for highly integrated gas sensors," Applied Physics B-Lasers and Optics **119**, 111–118 (2015).
10. L. Dong, A. A. Kosterev, D. Thomazy, and F. K. Tittel, "QEPAS spectrophones: design, optimization, and performance," Applied Physics B-Lasers and Optics **100**, 627–635 (2010).
11. H. Y. Lin, H. D. Zheng, B. Y. Antonio Z. Montano, H. P. Wu, M. Giglio, A. Sampaolo, P. Patimisco, W. G. Zhu, Y. C. Zhong, L. Dong, R, F. Kan, J. H. Yu, and V. Spagnolo, "Ppb-level gas detection using on-beam quartz-enhanced photoacoustic spectroscopy based on a 28 kHz tuning fork," Photoacoustics **25**, 100321 (2022).
12. K. Liu, X. Y. Guo, H. M. Yi, W. D. Chen, W. J. Zhang, and X. M. Gao, "Off-beam quartz-enhanced photoacoustic spectroscopy," Optics Letters **34**, 1594–1596 (2009).
13. P. Patimisco, A. Sampaolo, L. Dong, F. K. Tittel, and V. Spagnolo, "Recent advances in quartz enhanced photoacoustic sensing," Applies Physics Review **5**, 011106 (2018).
14. H. H. Lv, H. D. Zheng, Y. H. Liu, Z. F. Yang, Q. Wu, H. Y. Lin, B. Y. Antonio Z. Montano, W. G. Zhu, J. H. Yu, R. F. Kan, Z. Chen, and F. K. Tittel, "Radial-cavity quartz-enhanced photoacoustic spectroscopy," Optics Letters **46**, 3917-3920 (2021).
15. T. Milde, M. Hoppe, H. Tatenguem, M. Mordmüller, J. O'Gorman, U. Willer, W. Schade, and J. Sacher, "QEPAS sensor for breath analysis: a behavior of pressure," Applied Optics **57**, C120–C127 (2018).
16. Y. F. Ma, Y. He, X. Yu, C. Chen, R. Sun, and F. K. Tittel, "HCl ppb-level detection based on QEPAS sensor using a low resonance frequency quartz tuning fork," Sensors and Actuators B-Chemical **233**, 388–393 (2016).
17. H. P. Wu, A. Sampaolo, D. Lei, P. Patimisco, X. L. Liu, H. D. Zheng, X. K. Yin, W. G. Ma, L. Zhang, W. B. Yin, V. Spagnolo, S. T. Jia, and F. K. Tittel, "Quartz enhanced photoacoustic H_2S gas sensor based on a fiber-amplifier source and a custom tuning fork with large prong spacing," Applies Physics Letters **107**, 111104 (2015).
18. Y. F. Ma, Y. He, Y. Tong, X. Yu, and F. K. Tittel, "Quartz-tuning-fork enhanced photothermal spectroscopy for ultra-high sensitive trace gas detection," Optics Express **26**, 32103–32110 (2018).
19. X. N. Liu, S. D. Qiao, and Y. F. Ma, "Highly sensitive methane detection based on light-induced thermoelastic spectroscopy with a 2.3 μm diode laser and adaptive Savitzky-Golay filtering," Optics Express **30**, 1304–1313 (2022).
20. S. D. Russo, A. Zifarelli, P. Patimisco, A. Sampaolo, T. T. Wei, H. P. Wu, L. Dong, and V. Spagnolo, "Light-induced thermo-elastic effect in quartz tuning forks exploited as a photodetector in gas absorption spectroscopy," Optics Express **28**, 19074–19084 (2020).
21. Y. F. Ma, Y. Q. Hu, S. D. Qiao, Z. T. Lang, X. N. Liu, Y. He, and V. Spagnolo, "Quartz tuning forks resonance frequency matching for laser spectroscopy sensing," Photoacoustics **25**, 100329 (2022).
22. Q. D. Zhang, J. Chang, Z. H. Cong, and Z. L. Wang, "Quartz tuning fork enhanced photothermal spectroscopy gas detection system with a novel QTF-self-difference technique," Sensors and Actuators A-Physical **299**, 111629 (2019).
23. Z. T. Lang, S. D. Qiao, Y. He, and Y. F. Ma, "Quartz tuning fork-based demodulation of an acoustic signal induced by photo-thermo-elastic energy conversion," Photoacoustics **22**, 100272 (2021).
24. X. N. Liu, and Y. F. Ma, "Sensitive carbon monoxide detection based on light-induced thermoelastic spectroscopy with a fiber-coupled multipass cell," Chinese Optics Letters **20**, 031201 (2022).
25. T. T. Wei, A. Zifarelli, S. Dello Russo, H. P. Wu, G. Menduni, P. Patimisco, A. Sampaolo, V. Spagnolo, and L. Dong, "High and flat spectral responsivity of quartz tuning fork used as infrared photodetector in tunable diode laser spectroscopy," Applied Physics Reviews **8**, 041409 (2021).
26. S. D. Qiao, A. Sampaolo, P. Patimisco, V. Spagnolo, and Y. F. Ma, "Ultra-highly sensitive HCl-LITES sensor based on a low-frequency quartz tuning fork and a fiber-coupled multi-pass cell," Photoacoustics **27**, 100381 (2022).
27. X. N. Liu, S. D. Qiao, G. W. Han, J. X. Liang, and Y. F. Ma, "Highly sensitive HF detection based on absorption enhanced light-induced thermoelastic spectroscopy with a quartz tuning fork of receive and shallow neural network fitting," Photoacoustics **28**, 100422 (2022).
28. L. Hu, C. T. Zheng, M. H. Zhang, K. Y. Zheng, J. Zheng, Z. W. Song, X. Y. Li, Y. Zhang, Y. D. Wang, and F. K. Tittel, "Long-distance in-situ methane detection using near-infrared light-induced thermo-elastic spectroscopy," Photoacoustics **21**, 100230 (2021).
29. Y. M. Ma, C. T. Zheng, L. Hu, K. Y. Zheng, F. Song, Y. Zhang, Y D. Wang, and F. K. Tittel, "High-robustness near-infrared methane sensor system using self-correlated heterodyne-based light-induced thermoelastic spectroscopy," Sensors and Actuators B-Chemical **370**, 132429 (2022).
30. L. Hu, C. T. Zheng, Y. Zhang, J. Zheng, Y. D. Wang, F. K. Tittel, "Compact all-fiber light-induced thermoelastic spectroscopy for gas sensing," Optics Letters **45**, 1894-1897 (2020).
31. Y. F. Ma, Y. He, L. G. Zhang, X. Yu, J. B. Zhang, R. Sun, and Frank K. Tittel, "Ultra-high sensitive acetylene detection using quartz-enhanced photoacoustic spectroscopy with a fiber amplified diode laser and a 30.72 kHz quartz tuning fork," Applied Physics Letters **110**, 031107 (2017).
32. Q. Z. Wang, W. R.Wang, P. Patimisco, A. Sampaolo, and V. Spagnolo, "Fiber-ring laser intracavity QEPAS gas sensor using a 7.2 kHz quartz tuning fork," Sensors and Actuators B-Chemical **268**, 512–518 (2018).
33. Y. F. Ma, S. D. Qiao, P. Patimisco, A. Sampaolo, Y. Wang, and F. K. Tittel, and V. Spagnolo, "In plane quartz-enhanced photoacoustic spectroscopy." Applied Physics Letters **116**, 061101 (2020)
34. Z. J. Shang, S. Z. Li, B. Li, H. P. Wu, A. Sampaolo, P. Patimisco, V. Spagnolo, and L. Dong, "Quartz-enhanced photoacoustic NH3 sensor exploiting a large-prong-spacing quartz tuning fork and an

optical fiber amplifier for biomedical applications," Photoacoustics **26**, 100363 (2022).

35. Z. Wang, Q. Wang, H. Zhang, S. Borri, I. Galli, A. Sampaolo, P. Patimisco, V. L. Spagnolo, P. De Natale, and W. Ren. "Doubly resonant sub-ppt photoacoustic gas detection with eight decades dynamic range," Photoacoustics **27**, 100387 (2022).
36. Y. F. Ma, Y. He, P. Patimisco, A. Sampaolo, S. D. Qiao, X. Yu, F. K. Tittel, and V. Spagnolo, "Ultra-high sensitive trace gas detection based on light-induced thermoelastic spectroscopy and a custom quartz tuning fork." Applied Physics Letters **116**, 011103 (2020).
37. P. Patimisco, A. Sampaolo, H. Zheng, L. Dong, F. K. Tittel, and V. Spagnolo, "Quartz–enhanced photoacoustic spectrophones exploiting custom tuning forks: a review," Advances in Physics: X **2**, 169–187 (2017).
38. S. Dello Russo, A. Sampaolo, P. Patimisco, G. Menduni, M. Giglio, C. Hoelzl, V. M. N. Passaro, H. P. Wu, L. Dong, and V. Spagnolo, "Quartz-enhanced photoacoustic spectroscopy exploiting low-frequency tuning forks as a tool to measure the vibrational relaxation rate in gas species," Photoacoustics **21**, 100227 (2021).